

## RESEARCH PAPER

## THE IMPROVEMENT OF TENSILE PROPERTIES OF LOW-CARBON STEELS VIA SHORT-TIME INTERCRITICAL ANNEALING

*Meymanat Sadat Mohsenzadeh<sup>1\*</sup>*<sup>1</sup> Department of Materials and Metallurgical Engineering, University of Gonabad, Gonabad, Iran, P.O. Box 9691957678; [mohsenzadeh@gonabad.ac.ir](mailto:mohsenzadeh@gonabad.ac.ir)\*Corresponding author: [mohsenzadeh@gonabad.ac.ir](mailto:mohsenzadeh@gonabad.ac.ir), Department of Materials and Metallurgical Engineering, University of Gonabad, Gonabad, Iran, P.O. Box 9691957678

Received: 23.01.2023

Accepted: 11.03.2023

## ABSTRACT

The effect of low volume fraction formation of martensite on the tensile properties of low carbon steel was evaluated. First, steel samples with ferrite-cementite microstructure were produced. The thermomechanical treatment used included austenitizing at 1000 °C and then quenching in ice brine solution, tempering the obtained martensitic structure for 1 h at 650 °C, 80% cold rolling, and re-tempering for 2 h at 650 °C. In order to form a low volume fraction of martensite, steel samples with ferrite-cementite microstructure were intercritically annealed for 30 seconds at 740 °C. As a result of intercritical annealing treatment, 6.2% martensite was formed. The results of tensile test showed that the formation of 6.2% martensite led to the elimination of yield point phenomenon and Lüders banding, decrease of yield stress and increase of true stress at maximum load, while true uniform strain did not change significantly. The work hardening rate also increased significantly. Based on the results of modeling of the flow behavior with the Holloman equation, the work hardening capability of the steel sample including ferrite-cementite decreased after a certain plastic strain, while the work hardening capacity remained constant with the formation of a low volume fraction of martensite in the microstructure.

**Keywords:** low carbon steel; mechanical properties; martensite; short-time intercritical annealing

## INTRODUCTION

Low carbon steels are one of the most widely used materials in various industries due to their low cost and good formability. The result is that interest in these steels as a target for a wide range of studies aimed at improving their mechanical properties has not yet disappeared [1]. Increasing the strength of materials by forming an ultrafine grain (UFG) structure, has created new prospects for increasing the strength of low carbon steels and thus expanding their extent of applications. There is currently a lot of research work in this field. Severe plastic deformation (SPD) techniques such as equal channel angular pressing (ECAP), high pressure torsion (HPT) and constraint groove pressing have been used to produce ultrafine grain structures in low carbon steels [2-4]. Although the ultrafine grain low carbon steels produced have high strength, their ductility is severely reduced due to their poor work hardening capacity [5]. Cryorolling at the temperature of liquid nitrogen is a process in which severe strain is induced by applying relatively lower load to produce an ultrafine grain structure in the material [6]. 50% cryorolling of low carbon steel samples annealed at 550 °C resulted in significant grain refinement and increasing their yield and tensile strength [6]. Yuan et al. [7] proposed the process of cryorolling of martensite starting structure and then annealing to produce ultrafine grain low carbon steels. They proved that with this process a reasonable balance of strength and ductility is achieved. The dynamic recovery is suppressed during cryorolling. This leads to the formation of high density of defects and abundant nucleation sites for the ferrite grains. As a result, a UFG structure is formed after annealing of cryorolled martensitic steel. Some research has been conducted on the development of thermomechanical processes for the production of ultrafine grain

low carbon steels. Martensite treatment including cold deformation by plane strain compression followed by annealing has been used to produce nano/ultrafine grain low carbon steel [8]. It was reported that 91% cold rolling of dual phase starting microstructure including ferrite and martensite, and subsequent annealing below the eutectoid temperature, resulted in the production of ultrafine grain structure in low carbon steel [9]. Other processes used to produce ultrafine grain steel include bi-axial rolling at warm working temperature [10], asymmetric rolling with cone-shaped rolls at hot working temperatures [11], and severe warm rolling of low carbon steel [12]. It has been found that the addition of 0.028 wt% of niobium to ultrafine grain low carbon steel leads to a significant increase in strength without decreasing ductility [13]. In addition, niobium improves the thermal stability of ultrafine grain low carbon steel [14].

Although creating of ultrafine grain structure in low carbon steel increases the strength, it reduces the work hardening rate and uniform elongation. In addition, the ultrafine grain steels show the formation of Lüders bands during deformation, which is undesirable [15]. Therefore, other strategies such as creating a bimodal grain size distribution in ferrite have been used to improve the strength-ductility combination and eliminate the formation of Lüders bands [15]. Bahadur Singh et al. [5, 16] reported that the ductility of ultrafine grain steels produced by ECAP, can be significantly recovered by cold rolling and flash annealing at 600 °C. After flash annealing, a bimodal structure consisting of ultrafine and micron-sized ferrite grains are formed in low carbon steel. Such a structure has the suitable combination of strength-ductility. Electropulsing of ultrafine grain low carbon steel also leads to the formation of a structure with a bimodal grain size distribution in the ferrite, which can significantly recover the ductility of steel [14]. Ductility is recovered

due to the formation of micron-sized ferrite grain and a significant reduction in dislocation density. Coarsening of ultrafine grains into micron-sized grains occurs by the electromigration of high-angle grain boundaries [14]. The bimodal grain structure in low carbon steel was fabricated via deforming martensite starting structure by plane strain compression and then short-time annealing at high temperatures [17]. Using this method, the superior strength-ductility balance was obtained in comparison with the bimodal grain structures produced by the ferrite-martensite dual-phase starting microstructures. In order to improve the combination of strength and ductility, ultrafine grained heterostructured dual-phase (UFG-HSDP) steels including soft ferrite grains which are completely embedded in hard martensite grains, have been produced [1]. The proposed process involves cyclic annealing and cold rolling of martensitic steel in order to obtain a nano-lamellar microstructure followed by intercritical annealing for a short time.

Although many studies have been conducted to improve the mechanical properties of low carbon steels, the development of a process that is both economically and technologically efficient still needs further investigation. The present study is an attempt to improve the mechanical properties of low carbon steel through a simple process that is easily applicable. In this research, a low volume fraction of martensite phase was formed in a ferrite-spheroidized cementite microstructure by short-time intercritical annealing and its effect on the mechanical properties of low carbon steel was evaluated.

## MATERIAL AND METHODS

4.6 mm thick steel sheet was used in this study. The chemical composition of this steel was Fe-0.16 C-0.41 Si-1.15 Mn-0.018 P-0.01 S (wt.%). To produce the steel with ferrite-cementite microstructure (labeled "F-C" steel), samples with dimensions of 80×15 mm were cut from the sheet. After austenitizing at 1000 °C for 30 minutes in a laboratory box furnace, the samples were quenched in an ice brine solution to produce a fully martensitic structure. In order to facilitate the cold rolling of the samples, the martensitic structure was tempered at 650 °C for 1 hour and then cooled in water. After 80% of cold rolling by a laboratory rolling mill (the roll diameter of 57 cm), the samples were tempered again for 2 hours at 650 °C, and then cooled in water. In order to form a low volume fraction of martensite, a sample of the initial sheet after the previous steps was finally intercritically annealed at 740 °C for 30 seconds followed by quenching in ice brine solution. The sample prepared in this way is labeled the steel "F-C-M" throughout the paper.

For microstructural examination, the samples were mounted and after grinding and polishing, etched with 2% Nital solution (2 ml of nitric acid in 100 ml of alcohol). Microstructural examinations of the samples were performed with light microscopy and scanning electron microscopy. Micrographs of the etched samples were obtained using the Olympus BX60M Optical Microscope and the Leo 1450VP Scanning Electron Microscope (SEM). Quantitative analysis of microstructures was performed using Clemex image analysis software. Particle size of cementite, the size of martensite islands and the volume fraction of cementite phase as well as martensite phase were measured. At least 10 SEM micrographs were examined to determine each of the mentioned microstructural properties. Also, the grain size of ferrite in each sample was measured from at least 10 optical microscope images using Clemex software.

The deformation behavior of steels produced with two different of microstructures was investigated using the tensile test. Tensile specimens were prepared according to ASTM-E8 standard with a 25 mm gage length and were subjected to tensile test with a strain rate of 0.002 s<sup>-1</sup> by Zwick Z250 universal test machine.

## RESULTS AND DISCUSSION

**Fig. 1** shows the microstructure of the sample F-C. This sample contains 3.2% of cementite particles with an average size of 150 nm, which are uniformly distributed in the ferrite matrix. The average grain size of ferrite is 10 µm.

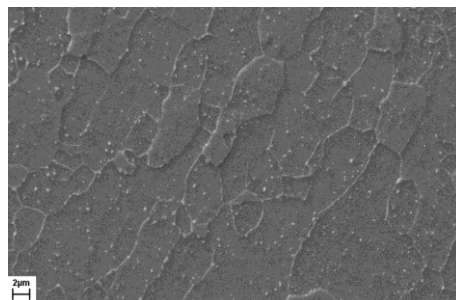


**Fig. 1** SEM micrograph representing the microstructure of F-C steel sample

The micrograph of the sample F-C-M is shown in **Fig. 2**. Intercritical annealing treatment at 740 °C for 30 seconds resulted in the formation of 6.2% of martensite islands with an average size of 1.73 µm. Martensite islands are mainly formed at the boundaries of ferrite grain. These islands are larger than cementite particles and have a mostly irregular morphology. In ferrite-cementite microstructures, the conditions for austenite nucleation (i.e. nucleation in carbon-rich regions and high-energy non-equilibrium defects) are met for cementite particles located at the boundaries of ferrite grains. Therefore, the interface between cementite particles and ferrite grain boundaries are the preferred nucleation sites for austenite during intercritical annealing [18]. Based on quantitative metallography results, the grain size of ferrite in the sample F-C-M was 10 µm, indicating that significant grain growth did not occur during short-time intercritical annealing. In addition, 1.8% of cementite particles with an average particle size of 150 nm remain in the microstructure.

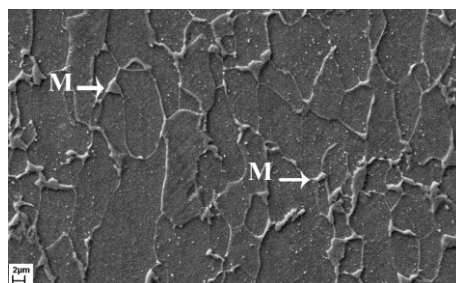


**Fig. 2** SEM micrograph representing the microstructure of F-C-M steel sample. M: martensite

**Fig. 3** shows the true stress-true strain curves of the samples F-C and F-C-M. The values of yield stress ( $\sigma_y$ ), true stress at maximum load ( $\sigma_u$ ) and true uniform strain ( $\epsilon_u$ ) for these samples are given in **Table 1**. As can be seen, the presence of fine cementite particles (diameter 150 nm) in the sample F-C increases  $\sigma_y$  compared to the ferritic steel ( $\sigma_y=301$  MPa [19]). On the other hand,  $\sigma_y$  of the sample F-C-M with microstructure including 6.2% martensite and 1.8% cementite, is in the range of ferritic steel,

as expected due to the effect of the martensite phase on decreasing the yield stress of dual phase steel [20]. Volume expansion due to the transformation of austenite islands to martensite causes internal stress in the ferrite matrix around the martensite island. This internal stress is the highest near the martensite-ferrite interface and gradually decreases with distance from the interface. The amount of internal stress close to the interface of martensite-ferrite is such that it causes the ferrite to yield within a certain range. Thus the internal stress in the plastic area is somewhat reduced, but nevertheless the internal stress in this area is higher than the surrounding area. By applying the stress in the tensile test, the internal stress promotes initial yielding, and the plastic flow begins with a stress lower than the ferrite yield stress without the presence of martensite islands. With the presence of martensite islands in the sample F-C-M,  $\sigma_u$  increased compared to the sample F-C while  $\epsilon_u$  is approximately equal to the sample F-C.

Yield point elongation can be seen in the stress-strain curve of the sample F-C (Fig. 3). The formation of 6.2% of martensite phase in the sample F-C-M resulted in the elimination of yield point elongation. In the sample F-C-M, internal stress induced plastic zones occupy a significant portion of the microstructure, and the unlocked dislocations associated with these zones are distributed over a larger area of the microstructure [21]. Therefore, under uniaxial tensile loading, yielding occurs in many areas and the formation of Lüders bands is prevented. It has been found that the formation of a bimodal grain size distribution in ferrite also causes the continuous yielding of steel [15, 22].

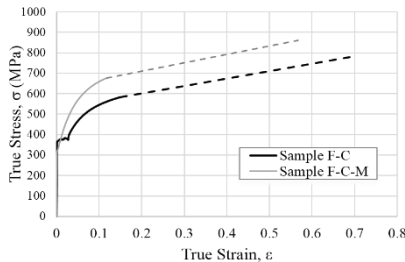


Fig. 3 The true stress-true strain curve of the samples F-C and F-C-M. The curves are plotted with dashed lines from neck to the final fracture point

Table 1 The values of yield stress ( $\sigma_y$ ), true stress at maximum load ( $\sigma_u$ ) and true uniform strain ( $\epsilon_u$ ) for the samples

Samples	$\sigma_y$ (MPa)	$\sigma_u$ (MPa)	$\epsilon_u$
F-C	404	583.5	0.12
F-C-M	308	677	0.116

Fig. 4 shows the changes of work hardening rate as a function of the true strain for the samples F-C and F-C-M, respectively. As can be seen, the work hardening rate of the sample F-C-M is significantly higher than that of the sample F-C.

Work hardening can be considered as the sum of the isotropic and kinematic hardening [23]. The isotropic hardening is due to the accumulation of barriers to dislocation motion as a result of the interaction of the dislocations with each other as well as with different microstructural components. The kinematic hardening is due to the back stress created by the accumulation of dislocation. The stress-strain curves of the samples F-C and F-C-M were modeled using a microstructure-based model. In this model, isotropic hardening was predicted taking into account the contributions of statistically stored dislocations (SSDs), geometrically necessary dislocations (GNDs), and Orowan dislocation

loops stored around the particles. The contribution of the second phase particles in the kinematic hardening was determined based on the Eshelby approach. The details of the model are described in the previous study [19]. Figs. 5a-b show the isotropic and kinematic hardening changes, respectively, as a function of the plastic strain for the studied samples. According to Figs. 5a-b, it is clear that the isotropic and kinematic hardening of the sample F-C-M are significantly higher than the sample F-C. Based on the modeling results, the density of dislocation loops stored around martensite particles in the sample F-C-M is higher than the density of dislocation loops stored around cementite particles in the sample F-C. Due to the larger size of martensite particles than cementite particles, the storage rate of dislocation loops around martensite particles is higher [19]. In addition, the length of the dislocation loops stored around the martensite particles is longer than that of the cementite particles. This means that despite the lower density of martensite particles than cementite particles, the density of dislocation loops stored around martensite particles is higher. As a result, the isotropic hardening of the sample F-C-M is significantly greater than that of the sample F-C (Fig. 5a).

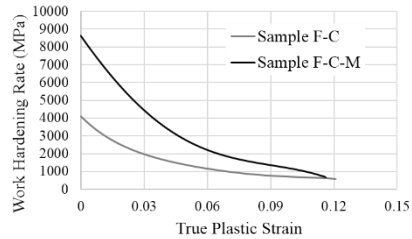
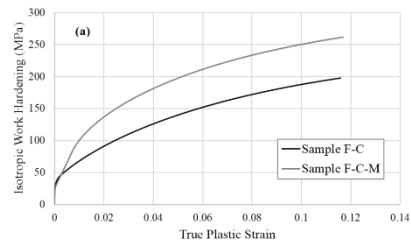
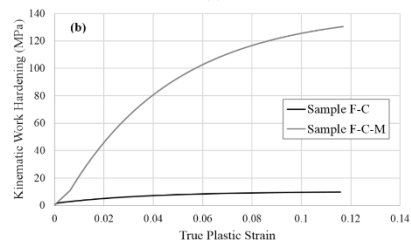


Fig. 4 The plot of work hardening rate as a function of plastic true strain for the studied samples (for sample F-C, the true plastic strain is equal to the necking strain minus the strain corresponding to the yield point elongation, and for sample F-C-M, the true plastic strain is equal to the necking strain minus the elastic strain)



(a)



(b)

Fig. 5 a) The isotropic work hardening as a function of true plastic strain, and b) The kinematic work hardening as a function of true plastic strain for the studied samples

Coarse particles, due to their higher misfit strain, create more internal stress than fine particles, and thus have a significant contribution to kinematic hardening [19]. Also, the kinematic contribution of work hardening is proportional to the volume fraction of the second phase particles. Therefore, in the sample F-C-M, due to the higher volume fraction of coarse martensite particles, the kinematic hardening is greater than in the sample F-C (Fig. 5b).

Although the formation of a bimodal grain size distribution in the ferrite prevents Lüders banding, it does not cause a significant change in the work hardening rate compared to the ultrafine grained structure [15]. However, according to the results of this study, the formation of a low volume fraction of martensite in the steel microstructure, in addition to preventing Lüders banding, leads to a significant increase in the work hardening rate.

The flow behavior of polycrystalline materials up to the point of maximum load can be described by the following equation known as the Holloman equation [24]:

$$\sigma = K\varepsilon^n \quad (1)$$

where:  $\sigma$  [MPa] - true stress  
 $\varepsilon$  - true strain  
 $n$  - strain hardening exponent  
 $K$  [MPa] - strength coefficient

The value of  $n$  indicates the tendency of the material to work hardening. The higher this tendency, the greater the value of  $n$ . The constants  $n$  and  $K$  are obtained by plotting stress and strain data on a logarithmic scale and fitting a line to them. The Holloman equation has been used in several studies to explain the work hardening behavior of steel [25]. In this study,  $n$  and  $K$  values were obtained using true stress and true strain data for the samples F-C and F-C-M. Plots of  $\ln\sigma$ - $\ln\varepsilon$  for the studied samples are shown in Fig. 6. The equation of the fitted line to the plot is also shown in the figure. The slope of the line determines the value of  $n$  and the width of the origin determines the value of  $K$ .

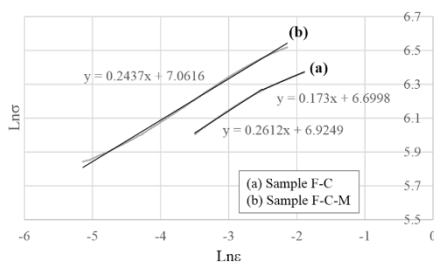


Fig. 6 Plots of  $\ln\sigma$ - $\ln\varepsilon$  for the studied samples.

According to the Holloman equation, two-stage work hardening is observed in the sample F-C and one-stage work hardening is observed in the sample F-C-M. Strain hardening exponent of the first stage of the sample F-C is 0.26, which is higher than the sample F-C-M ( $n=0.24$ ). The second stage of work hardening of the sample F-C starts from plastic strain of about 0.052. In the second stage, the value of  $n$  of the sample F-C is reduced to 0.17, which is significantly lower than that of the sample F-C-M. In the early stages of plastic deformation, the density of dislocation loops stored around the cementite particles in the sample F-C rapidly approaches the saturation value. As a result, after a certain amount of deformation, the work hardening capacity of this sample decreases due to the inability to accumulate dislocation loops around the particles. On the other hand, in the sample F-C-M, due to the presence of two types of particles, namely cementite and martensite, the contribution of moving dislocations

that reaches the particles is less than if there was only one type of particle in the microstructure. Thus, the rate by which the density of dislocation loops approaches the saturation value is lower than the sample F-C. Consequently, the ability to accumulate dislocation loops and work hardening capacity of the sample F-C-M remain constant during deformation. Based on the equation of the fitted line to the plot of  $\ln\sigma$ - $\ln\varepsilon$ , the strength coefficients ( $K$ ) of the sample F-C in the first and second stages of work hardening were obtained 1017.3 MPa and 812.23MPa, respectively. The values obtained are less than the strength coefficient of the sample F-C-M ( $K=1166.34$  MPa).

## CONCLUSION

In this study, the formation of low volume fraction of martensite was proposed to improve the mechanical properties of low carbon steel, and its effect on the tensile mechanical properties of low carbon steel was investigated. Formation of 6.2% martensite in steel with ferrite-cementite microstructure eliminated yield point phenomenon and Lüders banding, decreased the yield stress of steel from 404 MPa to 308 MPa, and increased true stress at maximum load from 583.5 to 677 MPa, while true uniform strain did not change significantly. Also, the work hardening rate of steel including low volume fraction of martensite, increases significantly. The presence of martensite particles in the microstructure increases isotropic and kinematic work hardening. The results of modeling the flow behavior using the Holloman equation predict a reduction of work hardening capacity after a certain plastic strain for the sample including ferrite-cementite, and a constant work hardening capacity after the formation of 6.2% martensite. In the sample including ferrite and cementite, due to the presence of one type of particle (cementite), the density of the dislocation loops stored around the particles quickly reaches saturation. As a result, after a certain amount of deformation, the work hardening capacity of this sample decreases due to its inability to accumulate dislocations around the particles. In the sample including ferrite, cementite and martensite, due to the presence of two types of particles (cementite and martensite), the contribution of mobile dislocations that reach the particles is less than if there was only one type of particle in the microstructure. As a result, the density of the dislocation loops stored around the particles slowly reaches saturation. Therefore, the ability to accumulate dislocations and thus the work hardening capacity of this sample remains constant during deformation.

## REFERENCES

1. J.X. Huang, Y. Liu, T. Xu, X. Chen, Q. Lai, L. Xiao, Z. Pan, B. Gao, H. Zhou, Y. Zhu: Materials Science and Engineering: A, 834, 2022, 142584. <https://doi.org/10.1016/j.msea.2021.142584>.
2. M. Karavaeva, S. Kiseleva, A. Ganeev, E. Protasova, M. Ganiev, L. Simonova, R. Valiev: Journal of materials science, 50, 2015, 6730-6738. <https://doi.org/10.1007/s10853-015-9227-2>.
3. F. Khodabakhshii, M. Haghshenas, H. Eskandari, B. Koohbor: Materials Science and Engineering: A, 636, 2015, 331-339. <https://doi.org/10.1016/j.msea.2015.03.122>.
4. R.B. Singh, N. Mukhopadhyay, G. Sastry, R. Manna: Metallurgical and Materials Transactions A, 48, 2017, 5449-5466. <https://doi.org/10.1007/s11661-017-4233-4>.
5. R.B. Singh, N. Mukhopadhyay, G. Sastry, R. Manna: Metallurgical and Materials Transactions A, 48, 2017, 1189-1203. <https://doi.org/10.1007/s11661-016-3892-x>.
6. Z.S. Aminah, M. Kanchana, A. Anasyida, H. Zuhailawati, M. Hiromi: Materials Today: Proceedings, 17, 2019, 1176-1182.

- <https://doi.org/10.1016/j.matpr.2019.06.560>.
7. Q. Yuan, G. Xu, M. Liu, S. Liu, H.-j. Hu: Transactions of the Indian Institute of Metals, 72, 2019, 741-749. <https://doi.org/10.1007/s12666-018-1526-2>.
8. S.M. Hosseini, A. Kermanpur, A. Najafizadeh, M. Alishahi: ISIJ international, 52, 2012, 464-470. <https://doi.org/10.2355/isijinternational.52.464>.
9. Y. Okitsu, N. Takata, N. Tsuji: Materials Science and Technology, 31, 2015, 745-754. <https://doi.org/10.1179/1743284714Y.0000000660>.
10. T. Inoue, R. Ueji, Y. Kimura: Materials Letters, 240, 2019, 172-175. <https://doi.org/10.1016/j.matlet.2019.01.007>.
11. T.K. Balgabekov, E.M. Azbanbayev, A.Z. Isagulov, D.A. Isagulova, N.B. Zakariya, N.Z. Yermaganbetov, A.R. Kenzhekeeva, Z.A. Konirova: Advanced Materials Research, Trans Tech Publications, 2015, 149-153. <https://doi.org/10.4028/www.scientific.net/AMR.1105.149>.
12. I.M. Safarov, A. Korznikov, R. Galeev, S. Sergeev, S. Gladkovskii, E. Borodin, I.Y. Pyshmintsev: The Physics of Metals and Metallography, 115, 2014, 295-302. <https://doi.org/10.1134/S0031918X14030107>.
13. Q. Zhang, Q. Yuan, Z. Wang, W. Qiao, G. Xu: Metallurgical and Materials Transactions A, 52, 2021, 5123-5132. <https://doi.org/10.1007/s11661-021-06459-3>.
14. Q. Zhang, Q. Yuan, Z. Wang, W. Qiao, G. Xu: steel research international, 93, 2022, 2100320. <https://doi.org/10.1002/srin.202100320>.
15. H. Azizi-Alizamani, M. Militzer, W.J. Poole: Scripta Materialia, 57, 2007, 1065-1068. <https://doi.org/10.1016/j.scriptamat.2007.08.035>.
16. R.B. Singh, N. Mukhopadhyay, G. Sastry, R. Manna: Materials Today: Proceedings, 26, 2020, 1514-1519. <https://doi.org/10.1016/j.matpr.2020.02.312>.
17. S. Hosseini, M. Alishahi, A. Najafizadeh, A. Kermanpur: Materials Letters, 74, 2012, 206-208. <https://doi.org/10.1016/j.matlet.2012.01.092>.
18. Q. Lai, M. Gouné, A. Perlade, T. Pardoën, P. Jacques, O. Bouaziz, Y. Bréchet: Metallurgical and Materials Transactions A, 47, 2016, 3375-3386. <https://doi.org/10.1007/s11661-016-3547-y>.
19. M.S. Mohsenzadeh, M. Mazinani: Materials Science and Engineering: A, 702, 2017, 113-124. <http://dx.doi.org/10.1016/j.msea.2017.06.093>.
20. T. Sakaki, K. Sugimoto, T. Fukuzato: Acta Metallurgica, 31, 1983, 1737-1746. [https://doi.org/10.1016/0001-6160\(83\)90172-4](https://doi.org/10.1016/0001-6160(83)90172-4).
21. M.S. Mohsenzadeh, M. Mazinani: Materials Science and Engineering: A, 673, 2016, 193-203. <http://dx.doi.org/10.1016/j.msea.2016.07.033>.
22. T. Wang, F. Zhang, M. Zhang, B. Lv: Materials Science and Engineering: A, 485, 2008, 456-460. <https://doi.org/10.1016/j.msea.2007.09.026>.
23. G. Fribourg, Y. Bréchet, A. Deschamps, A. Simar: Acta Materialia, 59, 2011, 3621-3635. <https://doi.org/10.1016/j.actamat.2011.02.035>.
24. J. Hollomon: AIME Transaction, 162, 1945, 268.
25. A. Zare, A. Ekrami: Materials Science and Engineering: A, 528, 2011, 4422-4426. <https://doi.org/10.1016/j.msea.2011.02.021>.